Molecular Biology of the Cell
Vol. 13, 3477–3492, October 2002

Localization of *Saccharomyces cerevisiae* Protein Phosphatase 2A Subunits throughout Mitotic Cell Cycle

Matthew S. Gentry and Richard L. Hallberg*

Department of Biology, Syracuse University, Syracuse, New York 13244

Submitted May 2, 2002; Accepted July 10, 2002
Monitoring Editor: Douglas Koshland

Protein phosphatase 2A (PP2A) regulates a broad spectrum of cellular processes. This enzyme is a collection of varied heterotrimeric complexes, each composed of a catalytic (C) and regulatory (B) subunit bound together by a structural (A) subunit. To understand the cell cycle dynamics of this enzyme population, we carried out quantitative and qualitative analyses of the PP2A subunits of *Saccharomyces cerevisiae*. We found the following: the level of each subunit remained constant throughout the cell cycle; there is at least 10 times more of one of the regulatory subunits (Rts1p) than the other (Cdc55p); Tpd3p, the structural subunit, is limiting for both catalytic and regulatory subunit binding. Using green fluorescent protein-tagged forms of each subunit, we monitored the sites of significant accumulation of each protein throughout the cell cycle. The two regulatory subunits displayed distinctly different dynamic localization patterns that overlap with the A and C subunits at the bud tip, kinetochore, bud neck, and nucleus. Using strains null for single subunit genes, we confirmed the hypothesis that regulatory subunits determine sites of PP2A accumulation. Although Rts1p and Tpd3p required heterotrimer formation to achieve normal localization, Cdc55p achieved its normal localization in the absence of either an A or C subunit.

INTRODUCTION

Protein phosphatase 2A (PP2A) is a major eukaryotic serine/threonine phosphatase playing an important role in a wide array of cellular processes, including DNA replication, RNA transcription, RNA splicing, regulation of translation, and cell cycle progression (Mumby and Walter, 1993; Schonthal, 1998; Millward *et al.*, 1999; Virshup, 2000; Janssens and Goris, 2001). PP2A is also an integral cellular target of invading toxins, parasites, and viruses (Millward *et al.*, 1999; Garcia *et al.*, 2000).

How PP2A can be involved in such a variety of different processes (i.e., presumably have so many different substrates) is attributable in great part to its structural plasticity. PP2A is a heterotrimer composed of a catlytic (C), structural (A), and regulatory (B) subunit; it is the multiplicity of regulatory subunits that primarily creates the extensive PP2A heterogeneity. For example, in mammals there are four separate classes of proteins that can furnish B function designated PR55 (B), PR61 (B′), PR72 (B″), and PR93/110 (B‴). Multiple isoforms exist within each B-type subunit class, leading to the potential of >40 different PP2A trimers. (reviewed in Janssens and Goris, 2001).

Although the complexity of PP2A in mammalian systems is considerable, PP2A complexity in *S. cerevisiae* is far simpler. The catalytic subunits are encoded by *PPH21* and *PPH22* (Ronne *et al.*, 1991), the structural subunit by *TPD3* (van Zyl *et al.*, 1989, 1992), and only two regulatory subunits by *CDC55* (a B-type) and *RTS1* (a B′-type). However, although *S. cerevisiae* has a much smaller repertoire of possible PP2A heterotrimers, mutations in the above-mentioned five genes elicit complex pleiotropic phenotypes. For example, although deletion of *PPH21* or *PPH22* alone produces no mutant phenotype, disruption of both generates cells that are temperature sensitive, have decreased growth rates, and exhibit cell wall and polarity defects (Ronne *et al.*, 1991; Lin and Arndt, 1995). Cells null for *TPD3* are temperature sensitive, exhibit RNA-processing defects, and become multibudded at low temperatures (van Zyl *et al.*, 1989, 1992). Finally, genetic analyses have shown that Cdc55p is required for maintaining bud morphology and proper cytokinesis (Healy *et al.*, 1991; Minshull *et al.*, 1996; Wang and Burke, 1997; Yang *et al.*, 2000), whereas Rts1p is necessary for regulating responses to a variety of stressful cellular conditions, for proper nucleus and spindle orientation, and for control of cyclin B2 degradation (Shu *et al.*, 1995, 1997; Yang and Hallberg, unpublished data).

Article published online ahead of print. Mol. Biol. Cell 10.1091/mbc.02–05–0065. Article and publication date are at www.molbiolcell.org/cgi/doi/10.1091/mbc.02–05–0065.

* Corresponding author. E-mail address: hallberg@syr.edu.

The question then becomes, How can such a small number of potentially different enzyme complexes affect so many different processes? We considered the answer to lie in previous suggestions (Sontag *et al.*, 1995; McCright *et al.*, 1996) that the role of the PP2A regulatory subunit might be to determine the cellular site to which a PP2A trimer is directed. For example, in mammalian cells certain regulatory subunits are found only in the nucleus or cytoplasm or associated with the cytoskeleton (reviewed in Janssens and Goris, 2001). Also, two alternate forms of PP2A B′ regulatory subunits in *Schizosaccharomyces pombe* accumulate at different cellular sites (Jiang and Hallberg, 2000; Le Goff *et al.*, 2001) and, more importantly, the sites of highest accumulation change during the cell cycle (Jiang and Hallberg, 2000; Le Goff *et al.*, 2001). Clearly, the act of sequestering a particular form of PP2A to a particular cellular site greatly limits the array of targets available to that PP2A trimer.

In this article, we have designed experiments to test directly the notion that a role of PP2A regulatory subunits is to determine the sites within the cell at which the structural and catalytic subunits become localized. To that end, using *S. cerevisiae* as our test system, we have created strains expressing single genes encoding green fluorescent protein (GFP)-tagged forms of each of the PP2A subunits and have examined their locations throughout the cell cycle. Also, strains were constructed that expressed a GFP-tagged subunit and at the same time were null for one or more of the other PP2A subunit genes. In this manner, we have been able to establish some of the "rules" by which the cell cycle-specific localization of different PP2A trimers is achieved.

MATERIALS AND METHODS

Strains, Plasmids, and Media

All strains used were derivatives of W303 and are listed in Table 1. Plasmids used are listed in Table 2. Details of strain and plasmid construction will be provided upon request. Standard yeast protocols and media were used (Rose *et al.*, 1990) as were recombinant DNA methodologies (Sambrook *et al.*, 1989). For microscopic visualization of fluorescently tagged proteins, cells were grown in YPD (1% yeast extract, 2% bactopeptone, 2% glucose) or synthetic media supplemented with the appropriate amino acids and 2% glucose and then washed and viewed in synthetic media with the appropriate amino acids and 2% glucose. To arrest cell growth nocodazole or hydroxyurea was added to a final concentration of 20 μg/ml and 0.2 M, respectively, for 3 h. In cases when pheromone was used for cell cycle arrest, cells were grown to OD_{600} 0.25 and α-factor was added at a final concentration of 1 μg/ml. In all cases, cells were microscopically examined (either by differential interference contrast for cell morphology or with 4,6-diamidino-2-phenylindole (DAPI) staining/fluorescence for nuclear morphology) throughout all experiments to ensure that cell cycle arrest had occurred and to ensure that cells were synchronous after arrest. When pheromone was used to induce shmoo formation, cells were grown to OD_{600} 0.25 and α-factor was added at a final concentration of 5 μg/ml. Yeast transformations were performed using lithium acetate as described previously (Kaiser *et al.*, 1994).

Complementation of Epitope and GFP-tagged Genes

Each epitope-tagged or GFP-tagged gene on a *CEN* plasmid was transformed into a strain carrying a null allele of the tagged gene. Each strain was tested under a variety of conditions specific for the gene in question to test the functionality of the tagged gene. Tagged genes that fully complemented the null allele were then chromosomally integrated, replacing the endogenous gene. These strains were then assayed under the same conditions used previously to test the functionality of the plasmid-borne tagged gene. Finally, the doubling time of each strain was compared with a wild-type strain. Only those tagged genes that passed all criteria showing wild-type characteristics were used in subsequent studies.

Determining Relative Concentrations of PP2A Subunits

Our approach to quantitation was to generate identically epitope-tagged forms of all five PP2A subunits as a possible means of comparing cellular protein levels. To that end, we generated genes tagged with the epitopes HA or HA_3 (influenza virus hemagglutinin), or MYC_{18} (human c-myc) at either their amino or carboxy terminus. We also generated some genes expressing the same or different epitopes at both termini. Using those genes that passed the complementation tests described above, we then determined the levels of each protein in a given strain by using the appropriate monclonal antibody (12CA5 for HA; 9E10 for MYC) and quantitative analysis of Western blots (see below). We found that regardless of the epitope used, and at which end of the protein to which it was attached, we calculated similar ratios of the various PP2A subunits (Figure 1, A–C; our unpublished data). Finally, to test for the possibility that the presence of epitopes might affect the turnover rates of the tagged proteins, we determined the cellular levels of differently epitope-tagged Tpd3p (Figure 1D) and Cdc55p (our unpublished data) by using antibodies specific for the two proteins. In all cases, the levels of the tagged proteins were essentially identical to those of the untagged forms.

DAPI Staining, Calcofluor Staining, FM4-64 Staining, and Microscopic Analysis

Staining cells with DAPI to determine their cell cycle stage was carried out as described previously (Pringle *et al.*, 1989). rho^O cells were used to visualize nuclei. The rho^O strains MSG92 and MSG96 were generated by treating cells with ethidium bromide as described previously (Guthrie and Fink, 1991). FM4-64 staining of vacuoles was carried out as described previously (Vida and Emr, 1995). Visualization of cells by differential interference contract microscopy was carried out on an Eclipse TE300 microscope (Nikon, Tokyo, Japan). Fluorescence of all cells was visualized on a BX60 microscope (Olympus, Tokyo, Japan) by using the appropriate filter set. Visualization of GFP or DAPI fluorescence was carried out using an enhanced green fluorescent protein (EGFP) or DAPI filter set (Chroma Technology, Brattleboro, VT), unless otherwise noted. Visualization of FM4-64 was carried out using the HQ:Texas Red filter set (Chroma Technology). Visualization of cyan fluorescent protein (CFP) fluorescence was carried out using the cyan GFP v2 filter set (Chroma Technology). The two-color imaging excitation and emission of fluorescent proteins was performed as described previously (Pearson *et al.*, 2001). Images were acquired using a charge-couple device camera (Olympus) with Magnafire software (Olympus) and analyzed using Photoshop (Adobe Systems, Mountain View, CA). Cells were prepared, sealed, and photographed in an agarose chamber for continuous time analysis of single cells as described previously (Tran *et al.*, 2001).

Protein Isolation, Electrophoresis, and Western Analysis

The extraction of total proteins by solubilizing cells in 1.8 M NaOH-5% β-mercaptoethanol, the separation of proteins by SDS-PAGE, and procedures used for Western analysis have been described previously (Shu and Hallberg, 1995; Shu *et al.*, 1997). Protein extracts containing MYC_{18} epitope-tagged subunits were separated using a 7% SDS-PAGE; all other protein extracts were separated

Table 1. Yeast strains

Strain	Genotype	Source or reference
MSG41	*MATα ade2-1 ura3-1 his3-11 trp1-1 leu2-3,112 HA_3:TPD3*	This study
MSG36	*MATα ade2-1 ura3-1 his3-11 trp1-1 leu2-3,112 HA_3:CDC55*	This study
YS69	*MATα ade2-1 ura3-1 his3-11 trp1-1 leu2-3,112 RTS1:HA_3*	Shu and Hallberg, 1995
MSG56	*MATα ade2-1 ura3-1 his3-11 trp1-1 leu2-3,112 MYC_{18}:TPD3*	This study
YS95	*MATα ade2-1 ura3-1 his3-11 leu2-3,112 cdc55::TRP1*	Shu *et al.*, 1997
MSG64	*MATα ade2-1 ura3-1 his3-11 trp1-1 leu2-3,112 RTS1:MYC_{18}*	This study
MSG39	*MATα ade2-1 ura3-1 his3-11 trp1-1 leu2-3,112 HA:TPD3*	This study
LH333	*MATα ade2-1 his3-11 trp1-1 leu2-3,112 pph22::URA3 HA:PPH21*	This study
LH337	*MATα ade2-1 ura3-1 trp1-1 leu2-3,112 pph21::HIS3 HA:PPH22*	This study
CY5488	*MATα ade2-1 ura3-1 his3-11 trp1-1tpd3::LEU2*	Di Como and Amdt, 1996
MSG23	*MATα ade2-1 ura3-1 his3-11 trp1-1 leu2-3,112 MYC:TPD3*	This study
MSG66	*MATα ade2-1 ura3-1 his3-11 trp1-1 leu2-3,112 GFP:TPD3*	This study
MSG96	*MATα ade2-1 ura3-1 his3-11 trp1-1 leu2-3,112 GFP:TPD3 rho^o*	This study
MSG167	*MATα ade2-1 ura3-1 his3-11 trp1-1 leu2-3,112 RTS1:GFP*	This study
MSG92	*MATα ade2-1 ura3-1 his3-11 trp1-1 leu2-3,112 RTS1:GFP rho^o*	This study
MSG136	*MATα ade2-1 ura3-1 his3-11 trp1-1 leu2-3,112 RTS1:GFP CFP:SPC42(TRP1)*	This study
JVK418	*MATα ade2-1 ura3-1 his3-1 trp1-1 leu2-3,112 ndo10-1*	Goh and Klimartin, 1993
MSG206	*MATα ade2-1 ura3-1 trp1-1 leu2-3,112 ndc10-1 RTS1-HA_3*	This study
MSG107	*MATα ade2-1 ura3-1 his3-11 trp1-1 leu2-3,112 GFP:CDC55*	This study
CY1145	*MATα ade2-1 trp1-1 leu2-3,112 pph21::HIS3 pph22::URA3*	Lin and Arndt, 1995
MSG81	*MATα ade2-1 ura3-1 his3-11 leu2-3,112 cdc55::TRP1 GFP:TPD3*	This study
MSG68	*MATα ade2-1 ura3-1 trp1-1 leu2-3,112 rts1::HIS3 GFP:TPD3*	This study
MSG148	*MATα ade2-1 ura3-1 trp1-1 leu2-3,112 pph21::HIS3 GFP:TPD3*	This study
MSG143	*MATα ade2-1 his3-11 trp1-1 leu2-3,112 pph22::URA3 GFP:TPD3*	This study
MSG139	*MATα ade2-1 trp1-1 leu2-3,112 pph21::HIS3 pph22::URA3 GFP:TPD3*	This study
AS21	*MATα ade2-1 ura3-1 cdc55::TRP1 tpd3::LEU2 rts1::HIS3*	This study
MSG4	*MATα ade2-1 ura3-1 trp1-1 tpd3::LEU2 pph21::HIS3*	This study
MSG11	*MAT□ ade2-1 his3-11 trp1-1 tpd3::LEU2 pph22::URA3*	This study
LH297	*MATα ade2-1 trp1-1 tpd3::LEU2 pph21::HIS3 pph22::URA2*	This study
MSG86	*MATα ade2-1 ura3-1 his3-11 leu2-3,112 cdc55::TRP1 RTS1:GFP*	This study
MSG100	*MATα ade2-1 ura3-1 his3-11 trp1-1 tpd3::LEU2 RTS1:GFP*	This study
MSG123	*MATα ade2-1 ura3-1 trp1-1 leu2-3,112 pph21::HIS3 RTS1:GFP*	This study
MSG126	*MATα ade2-1 his3-11 trp1-1 leu2-3,112 pph22::URA3 RTS1:GFP*	This study
MSG129	*MATα ade2-1 trp1-1 leu2-3,112 pph21::HIS3 pph22::URA3 RTS1:GFP*	This study
YS96	*MATα ade2-1 ura3-1 trp1-1 leu2-3,112 rts1::HIS3*	Shu *et al.*, 1997
AS11	*MATα ade2-1 ura3-1 trp1-1 rts1::HIS3 tpd3::LEU2*	This study
HFY3	*MATα ade2-1 ura3-1 leu2-3,112 rts1::HIS3 cdc55::TRP1*	Shu *et al.*, 1997
AS3	*MATα ade2-1 ura3-1 trp1-1 leu2-3,112 rts1::HIS3 pph21::HIS3*	This study
AS5	*MATα ade2-1 trp1-1 leu2-3,112 rts1::HIS3 pph22::URA3*	This study
AS8	*MATα ade2-1 trp1-1 leu2-3,112 rts1::HIS3 pph21::HIS3 pph22::URA3*	This study
AS13	*MATα ade2-1 ura3-1 his3-11 tpd3::LEU2 cdc55::TRP1*	This study
AS21	*MATα ade2-1 ura3-1 tpd3::LEU2 rts1::HIS3 cdc55::TRP1*	This study
MSG144	*MATα ade2-1 ura3-1 trp1-1 leu2-3,112 pph21::HIS3 GFP:CDC55*	This study
MSG146	*MATα ade2-1 his3-11 trp1-1 leu2-3,112 pph22::URA3 GFP:CDC55*	This study
MSG152	*MAT ade2-1 trp1-1 leu2-3,112 pph21::HIS3 pph22::URA3 GFP:CDC55*	This study
HFY21	*MATα ade2-1 leu2-3,112 cdc55::TRP1 pph21::HIS3 pph22::URA3*	Yang *et al.*, 2000
HFY17	*MATα ade2-1 ura3-1 leu2-3,112 cdc55::TRP1 pph21::HIS3*	Yang *et al.*, 2000
HFY19	*MATα ade2-1, his3-11 leu2-3,112 cdc55::TRP1 pph22URA3*	Yang *et al.*, 2000

using a 10% SDS-PAGE. The mouse monoclonal antibodies 12CA5 (Roche Applied Science, Indianapolis, IN) and 9E10 (Zymed Laboratories, South San Francisco, CA) were used to detect HA epitope-tagged proteins and MYC epitope-tagged proteins, respectively. Cdc28p and Pho85p were detected using the mouse PSTAIR monoclonal antibody (Sigma-Aldrich, St. Louis, MO). Tpd3p was detected using the rabbit anti-Tpd3p polyclonal antibody at 1:2000 (van Zyl *et al.*, 1992). Cdc55p was detected using the rabbit anti-Cdc55p polyclonal antibody at 1:3000 (Wei *et al.*, 2001). Visualization of protein concentration was done using alkaline phosphatase-conjugated secondary antibodies as described previously (Shu and Hallberg, 1995) or by using horseradish peroxidase-conjugated secondary antibodies and enhanced chemiluminescence as described previously (Jiang and Hallberg, 2000). When using enhanced chemiluminescence (Figure 1, A–C), multiple exposures of every Western blot were obtained both on film and by a Digital Science Image Station 440CF (Eastman Kodak, Rochester, NY). Signal intensities were quantified using Kodak Digital Science 1D software. The quantified signals from multiple exposures of each experiment were used to obtain the mean relative amounts and SDs. In each case, the value obtained from the signal of Tpd3p was divided into the value for the other subunits. A correction was then made for the relative masses of the different proteins to make comparisons at the level of the number of molecules. The

Table 2. Plasmids used

Name	Description[a]	Source or reference
pXH133	*SPC42-ECFP* fusion, *URA3*	He *et al.*, 2000
pJB130	MYC_{15}, *HIS3*	J. Baohant
314/PPH22	*PPH22*, *CEN* vector/*TRP1*	Lin and Ardnt, 1995
314/PPH21	*PPH21*, *CEN* vector/*TRP1*	Lin and Ardnt, 1995
pMG317	HA_3-*TPD3-MYC* fusion, *CEN* vector/*URA3*	This study
pMG119	*TPD3-MYC* fusion, *CEN* vector/*URA3*	This study
pMG79	*MYC-TPD3* fusion, *CEN* vector/*URA3*	This study
314/HA-PPH21	*HA-PPH21* fusion, *CEN* vector/*TRP1*	Lin and Ardnt, 1995
314/HA-PPH22	*HA-PPH22* fusion, *CEN* vector/*TRP1*	Lin and Ardnt, 1995
pMG354	*HA-GFP-PPH21* fusion, *CEN* vector/*TRP1*	This study
pMG437	MYC_{18}-*TPD3* fusion, *CEN* vector/*TRP1*	This study
pMG325	MYC_{18}-*TPD3* fusion, *CEN* vector/*URA3*	This study
LH283	*RTS1-*MYC_{18} fusion, *CEN* vector/*TRP1*	This study
pMG314	*RTS1-*MYC_{18} fusion, *URA3*	This study
pMG311	*RTS1-*MYC_{18} fusion, *CEN* vector/*LEU2*	This study
pMG369	*GFP(10A)-CDC55* fusion, *CEN* vector/*URA3*	This study
pMG348	MYC_{18}-*CDC55* fusion, *CEN* vector/*URA3*	This study
pMG429	MYC_{18}-*CDC55* fusion, *CEN* vector/*LEU2*	This study

[a] *CEN* plasmids are low copy; other plasmids do not have a yeast replication origin and were chromosomally integrated.

mean and SD for the relative protein amounts were obtained using Exel (Microsoft, Redmond, WA).

Chromatin Immunoprecipitation

Chromatin immunoprecipitation was performed as described previously (Meluh and Broach, 1999) with the following modifications. The percentage of cells exhibiting Rts1p-GFP or GFP-Tpd3p localized at kinetochores was enriched in hydoxyurea-arrested cells (our unpublished data). Cells were grown at 25°C to mid-exponential growth, arrested in 0.2 M hydoxyurea for 3 h at 25°C (25°C lysates) or for 1.5 h at 25°C, and then shifted to 37°C for 1.5 h (37°C lysates). Cells were fixed at 30°C in 1% formaldehyde for 2 h. The lysate from broken cells was sonicated six times at 30% for 10 s (chromatin sheared to an average size of 500 base pairs). The lysate was then centrifuged at 15,000 rpm for 5 min to remove debris, transferred to a new tube, and incubated overnight at 4°C with the appropriate antibody (1 μg of 3F10 anti-HA; Roche Applied Science; and 8 μg of 9E10 anti-MYC; Zymed Laboratories). To recover coimmunoprecipitated DNA, protein A-Sepharose beads were suspended in 175 μl of TE and 25 μl of elution buffer and incubated at 37°C for 3 h. The supernatant was collected and beads were suspended in 300 μl of elution buffer at 37°C for 2–3 h. To reverse cross-linking, lysates were incubated in 0.2 M NaCl at 65°C overnight; 1/20 of the immunoprecipitate and 1/40 of total chromatin were used as template for 21 cycles of PCR reactions with REDTaq DNA polymerase (Sigma-Aldrich). *CEN4* and *URA3* primers were used as described by He *et al.* (2001).

RESULTS

PP2A Subunit Stoichiometry

Before investigating the dynamics of PP2A subunits during the cell cycle, we felt it necessary to determine their relative stoichiometries. To that end, we constructed strains chromosomally expressing PP2A-encoding genes having either HA or MYC epitopes affixed to the C or N terminus (see MATERIALS AND METHODS). Each gene construct used complemented its respective null allele and, as shown below, the cellular levels of the tagged proteins was, in all cases examined, indistinguishable from the levels of their untagged, wild-type counterparts.

We first compared three strains expressing chromosomally integrated HA_3-*TPD3* (MSG41), HA_3-*CDC55* (MSG36), and *RTS1-*HA_3 (YS69). Figure 1A shows some of the data generated and a summary of the quantitative measurements. Normalizing protein levels of Tpd3p to 1.00 and correcting for mass differences, we calculated the relative amounts of Cdc55p and Rts1p to be 0.26 $\pm$ 0.06 and 3.58 $\pm$ 0.93, respectively. When strains expressing MYC_{18}-tagged forms of the same three genes were similarly analyzed (Figure 1B), the calculated ratios of the three proteins were 1.00 Tpd3p:0.29 $\pm$ 0.05 Cdc55p:2.80 $\pm$ 0.68 Rts1p. These data indicate that early log phase cells contain 10–14 times more Rts1p than Cdc55p. As a test of that prediction, we made serial dilutions of protein extracts of each of the strains expressing both identically tagged forms of Rts1p and Cdc55p and then carried out quantitative Western analyses. A 1:10 to 1:12 dilution of the Rts1p-HA_3 and Rts1p-MYC_{18} protein extracts gave approximately the same intensity as the signal from HA_3-Cdc55p and MYC_{18}-Cdc55p extracts, respectively (our unpublished data). Thus, there is indeed ~12 times more Rts1p than Cdc55p in early log phase cells.

We then analyzed in a similar manner HA-Tpd3p (MSG39), HA-Pph21p (LH333), and HA-Pph22p (LH337). These results showed (Figure 1C) that for every Tpd3p there was 3.41 $\pm$ 0.53 Pph21p, and 3.30 $\pm$ 0.57 Pph22p. Our finding an equivalence of Pph21p and Pph22p confirms previous reports (Di Como and Arndt, 1996). Finding an excess of catalytic subunits relative to Tpd3p was not unexpected given that both Pph21p and Pph22p can assemble into other complexes (Di Como and Arndt, 1996; Jiang and Broach, 1999).

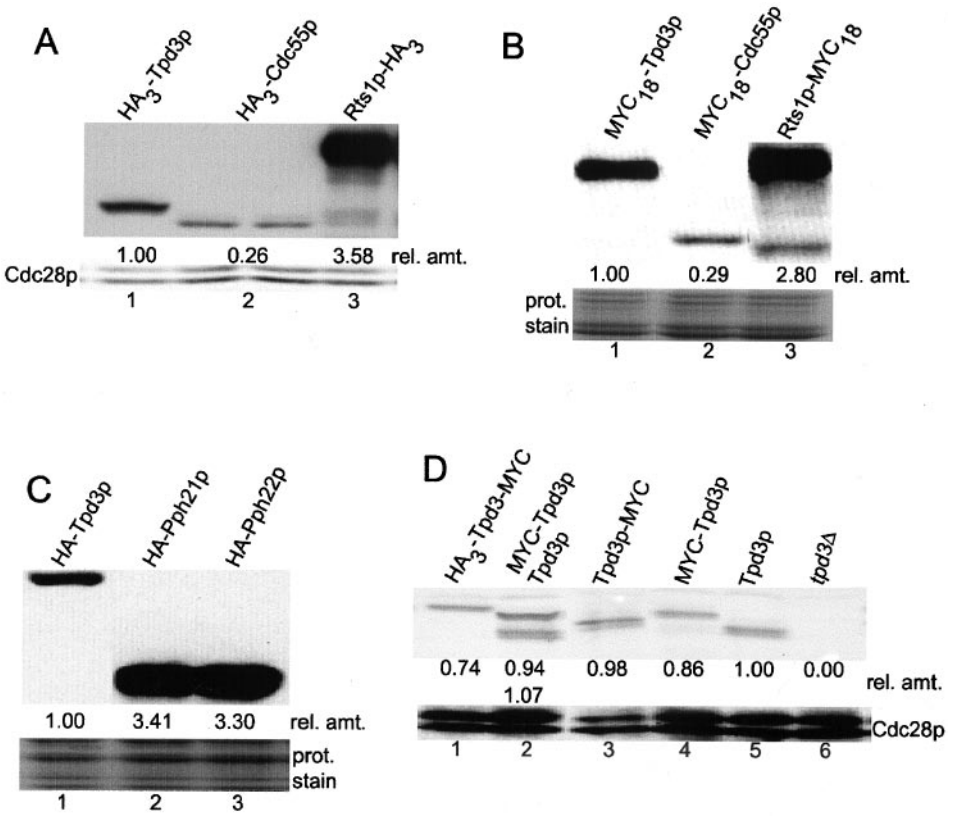

Figure 1. Determining the relative concentrations of the five different PP2A subunits. Strains expressing epitope-tagged *TPD3*, *CDC55*, *RTS1*, *PPH21*, and *PPH22* (see MATERIALS AND METHODS for details) were grown at 30°C to early log phase. Total cell proteins were isolated, separated by SDS-PAGE, transferred to nitrocellulose filters, and immunodecorated with the appropriate monoclonal antibody. Quantitative analyses using chemiluminescence were carried out as described in MATERIALS AND METHODS. All values for the relative amounts (rel. amt.) of a given subunit are expressed as a ratio of the number of molecules of that particular protein subunit to the number of Tpd3p molecules, which is set to 1.0. Loading controls either show that portion of a gel that had not been transferred but stained with Coomassie blue (B and C) or show Cdc28p visualized on the filter by using anti-PSTAIR antibody (A and D). (A) HA_3-tagged proteins. Top, proteins were immunodecorated with 12CA5 anti-HA. Lane 1, HA_3-Tpd3p from MSG41; lanes 2 and 3, HA_3-Cdc55p from MSG36; lane 4, Rts1p-HA_3 from YS69. This is a representative blot from 22 exposes from six experiments. (B) MYC_{18}-tagged proteins. Top, proteins were immunodecorated with 9E10 anti-MYC. Lane 1, MYC_{18}-Tpd3p from MSG56; lane 2, MYC_{18}-Cdc55p from YS95 with pMG348; lane 3, Rts1p-MYC_{18} from MSG64. This is a representative blot from 15 exposes from five experiments. (C) HA-tagged proteins. Top, proteins were immunodecorated with 12CA5 anti-HA. Lane 1, HA-Tpd3p from MSG39; lane 2, HA-PPh21p from LH333 containing pRS314 *PPH22*; lane 3, HA-Pph22p from LH337 containing pRS314 *PPH21*. This is a representative blot from 12 exposes from four experiments. (D) Detection of levels of normal and epitope-tagged forms of Tpd3p. Top, Tpd3p was immunodecorated with anti-Tpd3p. The relative amounts were calculated from five experiments. This is a representative blot. Lanes 1, 3, 4, and 6 are CY5488 expressing HA_3-Tpd3p-MYC (pMG317), Tpd3p-MYC (pMG119), MYC-Tpd3p (pMG79), or no Tpd3p, respectively; lanes 2 and 5 are W303 cells expressing MYC-Tpd3p (pMG79) or Tpd3p, respectively.

It was possible that a tagged protein could have an altered turnover rate and hence affected the level of that protein relative to a wild-type form. We thus compared the protein levels of a number of differently tagged subunits with the level of an untagged subunit and found that the cellular levels of amino-terminal–tagged Tpd3p, carboxy-terminal–tagged Tpd3p, and Tpd3p tagged at both termini were all similar to the level of untagged Tpd3p (Figure 1D). Similar results were obtained using an anti-Cdc55p antibody (courtesy of E. Ogris) and variously tagged *CDC55* constructs (our unpublished data). Thus, degradation rates of the epitope-tagged proteins were not altered.

We concluded that 1) epitope-tagged subunits can yield an accurate measurement of relative protein abundance; 2) there is a significant excess of both regulatory (B plus B′) subunits and catalytic (C) subunits relative to Tpd3p (the A subunit); 3) at no time can all Rts1p be a part of a PP2A trimer; 4) at any given time a maximum of one-seventh of all catalytic subunits can be associated with Tpd3p; and 5) some mechanism must operate to permit Cdc55p to effectively compete with Rts1p for binding to the AC dimer.

PP2A Subunit Localization Methodology

For localization studies we used the same strategy used for the quantitation studies, namely, GFP tag each PP2A gene, replace the chromosomal gene with the GFP-tagged version (with its normal promoter), and use only those strains exhibiting wild-type behavior. We then used two methods to assess whether there were any cell cycle-dependent localizations of PP2A subunits. In the first case, we grew cells in YPD to early log phase and microscopically examined a representative sample of all cells in the asynchronous population. Cells were divided into classes based on cell cycle morphology: nonbudded, small/medium budded, large budded with one nucleus, and large budded with two nuclei. Each class was scored for either having or lacking a characteristic localization pattern of a particular subunit. The percentage of cells in each class showing the trademark localization pattern was calculated. Alternatively, we grew cells to early exponential phase in YPD, arrested them with nocodazole or α-factor for 3 h, washed them into fresh medium, and then photographed cells at 15-min intervals

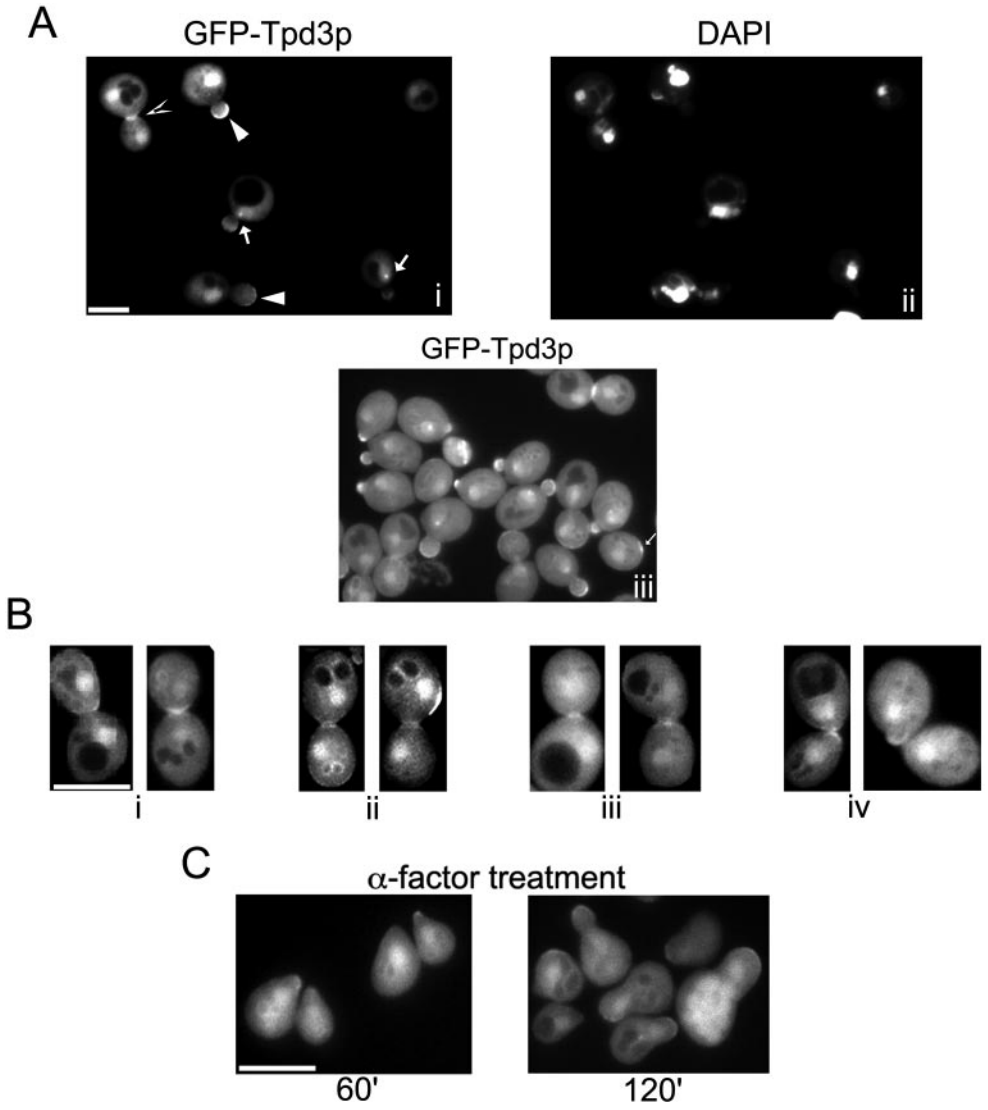

Figure 2. GFP-Tpd3p localization. GFP-Tpd3p fluorescence was visualized in MSG66 or MSG96 cells grown at 30°C to early log phase. In this and subsequent figures, large arrows denote kinetochore/SPB fluorescence; small arrows denote the presumptive bud site and/or the new cell wall of post-telophase cells; closed arrowheads denote bud tip fluorescence; open arrowheads denote bud neck fluorescence; bars, 5 μm. (A) MSG96 cells grown in the presence (i and ii) or absence (iii) of 1 μg/ml DAPI for 1 h, to visualize DNA. Cells were examined microscopically and photographed using EGFP (i and iii) or DAPI (ii) filter sets (Chroma Technology). (B) Time-lapse microscopy was performed using MSG66 cells (see MATERIALS AND METHODS). Seven individual cells were photographed starting when GFP-Tpd3p was first seen at the bud neck and then photographed every 2 min for 20–34 min. i–iv are representative cells from these experiments. (C) Localization of Tpd3p in premating cells. MSG66 cells were grown to early log phase, treated with 5 μg/ml α-factor for 60 and 120 min, and photographed.

over a 3-h period. Quantitation of cellular localization patterns of PP2A subunits was the same as with the first method. Both methods generated essentially the same results. Because we photographed cells to score localizations, in each photograph a certain percentage of cells with a trademark localization pattern was not in focus. Thus, our reported percentages for localization are conservative and never reach 100%.

PP2A Subunit Localizations

GFP-Tpd3 was found in the cytoplasm and nucleus of cells in all cell cycle stages (Figure 2A, i and ii). It was seen concentrated in a crescent shape at the bud tip of small/medium budded cells and in cells with the smallest visible bud (Figure 2A, closed arrowheads). In small/medium budded cells, GFP-Tpd3p localized to a bright spot (large arrows) in or adjacent to the nucleus. This spot appeared in cells in which the nucleus had migrated toward the bud neck, but before nuclear division was visible. We assumed it most likely to be at the spindle pole body (SPB) and attempted to determine whether GFP-Tpd3p colocalized with CFP-Spc42, a SPB component (Donaldson and Kilmartin, 1996). Unfortunately, due to the strong nuclear signal of GFP-Tpd3p, we were unable to confirm or disprove this assumption. However, we later show that Rts1p does, in fact, colocalize with Spc42p and that the localization of Tpd3p to this perinuclear spot requires the presence of Rts1p (see below).

GFP-Tpd3p also accumulated at the bud neck of post-telophase cells (Figure 2, A and B). This localization changed (Figure 2B, i–iv) as cells progressed from mitosis through cytokinesis. (To determine the kinetics of localization changes we used continuous microscopy of single cells; see MATERIALS AND METHODS.) Tpd3p was first found on the daughter side of the bud neck (Figure 2B, i) and then at the neck as two rings (Figure 2B, ii). Just before cytokinesis,

Tpd3p was concentrated in a tight single band at the juncture between the mother and bud (Figure 2B, iii), and then, after cell separation, it was seen at the new cell wall of just one of the postdivisional cells (Figure 2B, iv). Finally, GFP-Tpd3p became localized at the presumptive bud site of one of the newly formed nonbudded cells (Figure 2A, iii, small arrow).

Because some proteins that are known to localize to newly emerging buds also show accumulation at the polarized tips of premating cells ("shmoos"), we asked whether Tpd3p also exhibited this behavior. We found that essentially all cells treated with mating pheromone, when examined after 60 and 120 min, had GFP-Tpd3p localized as a crescent at the shmoo tip. Consistent with this finding is the fact that *tpd3*Δ cells treated with pheromone have abnormal mating projections and display a reduced mating efficiency (our unpublished data). Thus, it is most likely that localized PP2A activity is required for proper polarized growth in both normal cell division and in the mating process.

Rts1p-GFP appeared in the cytoplasm and nucleus in all cell cycle stages (Figure 3A, i and ii), but the relative intensity of the nuclear signal was far less pronounced than the nuclear signal of GFP-Tpd3p (Figures 2A and 3A). Rts1p-GFP was localized as a bright spot (large arrows) in or adjacent to the nucleus in 70% of small/medium budded cells (Figures 3A and 6). As with Tpd3p, perinuclear localization of Rts1p-GFP occurred after the nucleus had migrated toward the bud and before visible nuclear division. Rts1p-GFP was also seen at the bud neck (open arrowheads) in 45% of post-telophase cells (Figures 3A and 6). Rts1p-GFP localization at the bud neck was dynamic and similar to the GFP-Tpd3p localization (Figure 3B, i–iii). As before, to determine the kinetics of its localization at the bud neck, we followed Rts1p in single cells. Rts1p-GFP was first seen on the bud side (Figure 3B, i); then in the middle, occasionally as two rings (Figure 3B, ii); and finally, as a single band between the mother and daughter (Figure 3B, iii). Unlike Tpd3p, however, Rts1p-GFP was never seen at the bud neck in cells in the latest stages of cytokinesis, in cells that had just completed cytokinesis, or at new bud sites.

To determine whether Rts1p-GFP was localized at a SPB, we constructed a strain (MSG136) expressing both *RTS1:GFP* and *CFP:SPC42* and found that Rts1p-GFP and CFP-Spc42p colocalized after SPBs migrated toward the bud but before the duplicated SPBs begin to separate (Figure 3C, i–iii). At this time, centromeres are proximal to the SPBs (Goh and Kilmartin, 1993; Jin *et al.*, 1998). Given that the Rts1p-GFP spot often seemed significantly larger than the CFP-Spc42p spot, we considered that Rts1p-GFP might actually be localized at the kinetochores near the SPBs. This indeed seemed to be the case. As the SPBs separated, Rts1p-GFP was found between the two SPBs as a single dot (Figure 3C, iv and v) or in a bilobed pattern (Figure 3C, vi) in a manner previously described for kinetochore components (He *et al.*, 2000, 2001). As the SPBs moved further apart, Rts1p-GFP was then seen as two dots between the SPBs (Figure 3C, vii), a pattern also seen for bone fide kinetochore proteins (He *et al.*, 2000, 2001). The concentration of Rts1p in the nucleus remained relatively high throughout karyokinesis, and it was only after complete nuclear separation that Rts1p then began its accumulation at the bud neck.

Although the pattern of Rts1p localization was highly suggestive of a kinetochore association, to test that directly we performed a chromatin immunoprecipitation (ChIP) analysis. *NDC10* encodes a protein that is part of the CBF3 complex that is required for kinetochore assembly and maintenance (Goh and Kilmartin, 1993). In an *ndc10-1* strain, the kinetochore complex disassembles at 37°C (Goh and Kilmartin, 1993). We constructed strains carrying both an *ndc10-1* gene and an *RTS1:HA*$_3$ gene and then determined whether an immunoprecipitation of HA-tagged Rts1p would coprecipitate chromatin-associated centromeric DNA (*CEN4*) when the kinetochore was intact (at 25°C) but not when it had been disassembled (at 37°C). This turned out to be the case (Figure 3D). In negative controls in which the Rts1p was not tagged, no centromeric DNA was precipitated. As a control for the specificity of the DNA precipitated, we examined the precipitate for a DNA sequence that is not present at the centromere (*URA3*) and found none (Figure 3D). Similar results were obtained using MYC$_{18}$-Tpd3p (our unpublished data). Therefore, Rts1p-HA$_3$ and MYC$_{18}$-Tpd3p are both bound to centromeric DNA in a CBF3-dependent manner.

As with both Rts1p and Tpd3p, GFP-Cdc55p localized to the nucleus in >90% of all cells, albeit at a reduced intensity compared with the other two. GFP-Cdc55p localized to the bud tip of the smallest visible buds, to the bud tip of small/medium budded cells, and to some buds that were nearly as large as the mother (Figure 4A, closed arrowheads). It also localized to the bud neck (Figure 4A, open arrowheads) in 53% of post-telophase cells (Figure 6). GFP-Cdc55p was seen on the daughter side of the bud neck (Figure 4B, i), as a ring at the bud neck (Figure 4B, ii), as two rings at the bud neck (Figure 4B, iii), and at the new cell wall of one of the two buds that were completing cytokinesis (Figure 4B, iv). Finally, GFP-Cdc55p localized to what seemed to be the presumptive bud site and/or the postcytokinesis new cell wall of cells completing or just having completed cytokinesis (Figure 4A, small arrows). Thus, it showed an identical localization pattern to that observed for Tpd3p.

GFP-Cdc55p also showed significant localization at what seemed to be vacuoles in cells of all cell cycle stages (Figure 4A). FM4-64 is a vital stain that stains the vacuolar membrane and can be visualized with fluorescence microscopy (Vida and Emr, 1995). When *GFP-CDC55* cells were stained with FM4-64, GFP-Cdc55p colocalized with the stain in cells in all cell cycle stages (Figure 4C). A closer examination of GFP-Tpd3p localization showed a relatively weak signal at vacuolar membranes as well (our unpublished data). Thus, some PP2A is vacuolar membrane associated throughout the cell cycle.

Because GFP-Cdc55p, like Tpd3p, localized to the polarized bud tip we examined GFP-Cdc55p localization in pheromone-treated cells. In cells treated with mating pheromone for 60 or 120 min, GFP-Cdc55p also localized to the shmoo tip in a pattern identical to that shown by Tpd3p (Figure 4D).

Finally, we examined the subcellular localization of Pph21p and Pph22p. Initially, we determined Pph21p and Pph22p localization by immunofluorescence with a strain expressing an HA-tagged *PPH21* or *PPH22* that fully complemented the *pph21*Δ*pph22*Δ (CY1145) null phenotype. The immunofluorescence data showed that Pph21p and Pph22p

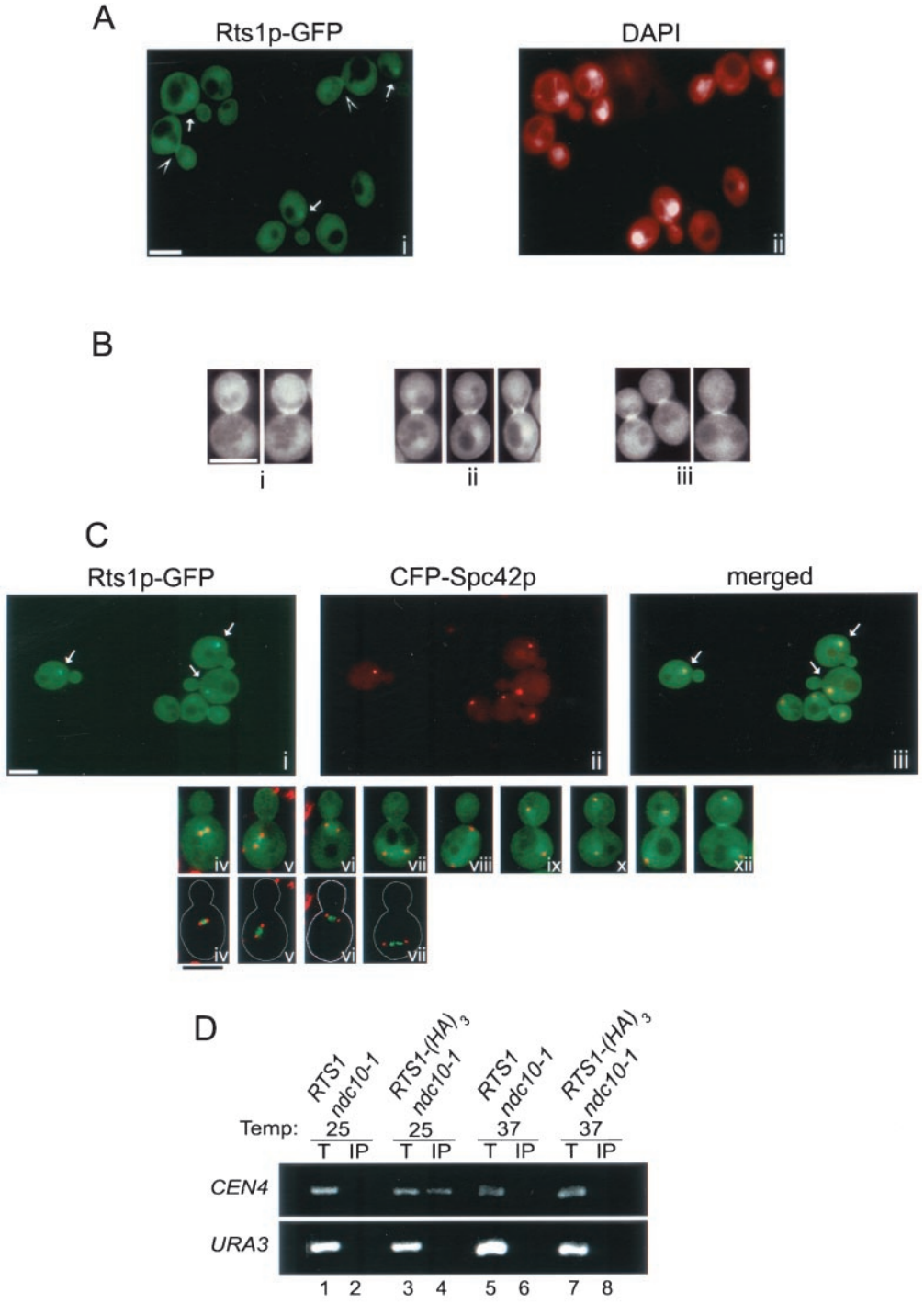

Figure 3. Rts1p-GFP localization. All cells were treated and analyzed as in Figure 2. (A) MSG92 cells were grown in the presence of DAPI as described for GFP-Tpd3p. Cells were photographed using EGFP (i) or DAPI (ii) filter sets (Chroma Technology). (B) Time-lapse microscopy was performed using MSG167 cells. Five individual cells were photographed starting when Rts1p-GFP was first visible at the bud neck and then every 2 min for 12–20 min. i–iii are representative cells from these experiments. (C) Rts1p-GFP and CFP-Spc42p fluorescence from MSG136 cells was photographed using yellow GFP and cyan GFP v2 filter sets (Chroma Technology), respectively. The two images were merged using Photoshop (iii–xii). iv–xii show cells at different stages of spindle elongation. Bottom, iv–vii have had their background green fluorescence reduced to a minimum to enhance the localization of Rts1p-GFP. (D) Anti-HA ChIP assays (see MATERIALS AND METHODS) were performed on *RTS1* (JVK418) or *RTS1-HA*$_3$ (MSG206) *ndc10-1* cells arrested in 0.2 M hydoxyurea for 3 h. ChIP analysis was performed with extracts of both strains at 25 and 37°C. The templates used for PCR were DNA from total chromatin (T) or DNA brought down in the anti-HA immunoprecipitate (IP). Primers used were designed to amplify *CEN4* and *URA3* DNA.

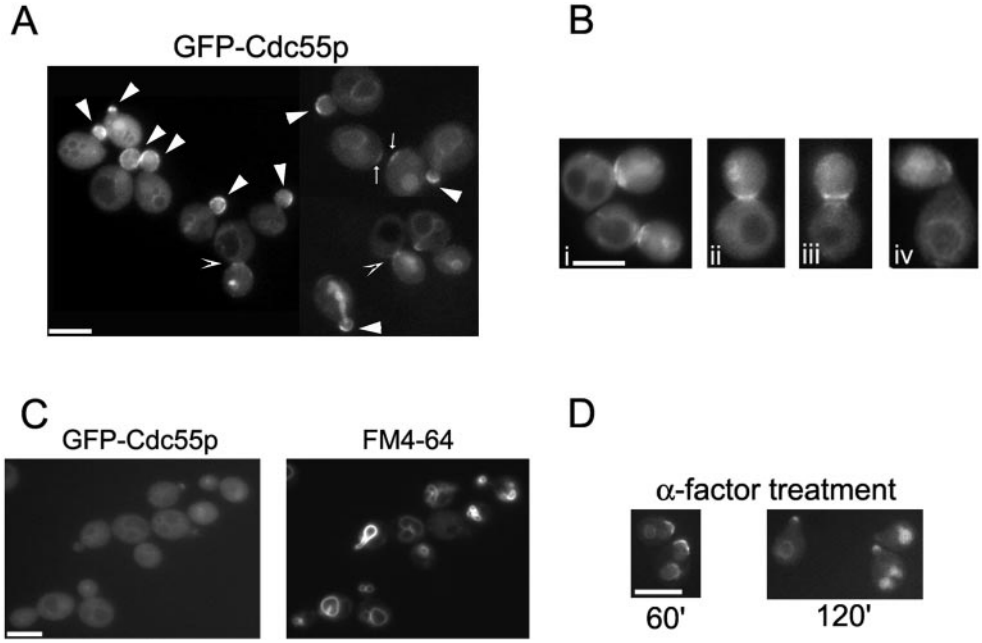

Figure 4. GFP-Cdc55p localization. (A and B) MSG107 cells were grown and examined as described in Figure 2. (C) MSG107 cells were grown in YPD, stained with 20 μM FM4-64 for 30 min, and microscopically examined using EGFP and HQ:Texas Red filter sets (Chroma Technology) to visualize GFP-Cdc55p and vacuolar staining, respectively. (D) Localization of Cdc55p in premating cells. MSG107 cells were grown in YPD, treated with 5 μg/ml α-factor for 60 and 120 min, and photographed.

were uniformly distributed in the cytoplasm and highly concentrated in the nucleus (our unpublished data). We then GFP tagged *PPH21* and although the *GFP-PPH21* construct did not fully complement its null allele (our unpublished data), the distribution of Pph21p gave similar results to our immunofluorescence experiments. In addition to nuclear and cytoplasmic localization, GFP-Pph21p was also observed at the bud tip of small and medium budded cells (Figure 5, closed arrowheads), as a faint perinuclear spot (Figure 5, arrows), and at the bud neck of post-telophase cells (Figure 5, open arrowheads). However, localization of Pph21p at bud tips, the bud neck, or the kinetochore was rarely observed, but because *GFP-PPH21* did not complement the null allele, these observations are not necessarily that surprising.

Tpd3p Is Dependent on B and C Subunits to Establish and/or Maintain Normal Localization Patterns

To begin to understand the "rules" regarding the necessity, or lack thereof, of particular subunits in directing the localization of other PP2A subunits, we first examined the effects of deleting individual PP2A subunit-encoding genes on the localization of Tpd3p. In all cases, we developed strains encoding GFP-Tpd3p and also deleted for one of the other PP2A-encoding genes. (It should be emphasized that if we find abnormal accumulations of a particular subunit, we cannot distinguish between the loss of targeting of that subunit or the inability to maintain an accumulation at its cellular location.)

In *cdc55*Δ cells (MSG81) GFP-Tpd3p maintained its cytoplasmic distribution and nuclear localization in all cell cycle stages, but the relative intensity of the nuclear localization was diminished (Figure 7A). Normal localization to the kinetochore (large arrows) in small/medium budded cells occurred, and although bud neck localization was still observed (open arrowheads), it was at a reduced frequency (42 vs. 61%) in post-telophase cells (Figure 7, A and E). Most strikingly, in *cdc55*Δ cells, GFP-Tpd3p was rarely found at bud tips, being seen in <5% of small/medium budded cells compared with 70% in wild-type cells (Figure 7E).

In *rts1*Δ cells (MSG68) GFP-Tpd3p was still found in the cytoplasm, but there was a sharp increase in its relative nuclear staining (Figure 7, B and E). Although it was still found at the bud tips of small/medium budded cells and at the bud neck of post-telophase cells, GFP-Tpd3p was there at a reduced frequency and a decreased intensity. In contrast, no GFP-Tpd3p was seen at the kinetochores in these cells (Figure 7, B and E). Thus, there is an absolute requirement for Rts1p for Tpd3p localization at the kinetochore, and although Tpd3p can still be directed to the bud neck and bud tip in the absence of Rts1p, the maintenance of wild-type levels at these locales also requires the presence of Rts1p.

In cells in which both *CDC55* and *RTS1* were disrupted, Tpd3p was never found at the bud neck, the emerging bud periphery, or the kinetochore (our unpublished data). It was, however, more concentrated in the nucleus. This is consistent with the localization patterns found in the single knockout strains and clearly indicates that Tpd3p bud neck localization is directed by both Cdc55p and Rts1p. Whether the initial timing of Tpd3p localization and the specific sites of accumulation directed by the B and B′ subunits differ remains to be determined.

In strains in which one or the other of the C-encoding subunits was deleted, the results were the same: GFP-Tpd3p localized to the kinetochore, the bud neck, and the emerging bud tips, albeit at a reduced frequency and usually at a reduced intensity (Figure 7, C and E). In contrast, in a *pph21*Δ*pph22*Δ strain, localization of GFP-Tpd3p to these

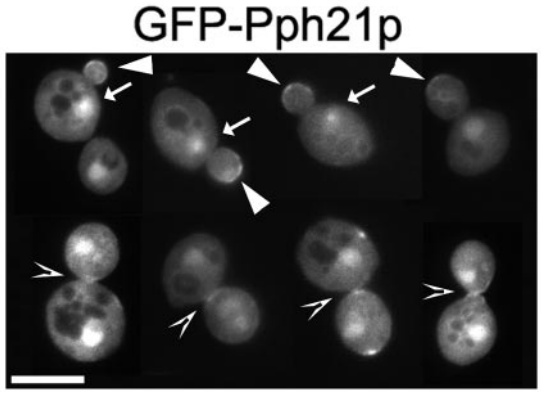

Figure 5. GFP-Pph21p localization. CY1145 cells carrying the plasmid pMG354 were grown and examined as described in Figure 2.

same three sites was essentially abolished, although a strong nuclear signal was still evident along with a uniform cytosolic staining (Figure 7D). These data would indicate that if a PP2A heterotrimer cannot be formed, Tpd3p cannot be directed to, and/or be maintained at, any of the cell cycle-specific sites at which it normally accumulates.

One possible explanation for the preceding results would be that Tpd3p is more subject to ectopic degradation when other subunits are not present. The changes in localization patterns could then be the result of selective degradation of Tpd3p rather than the loss of localization. To address this possibility, we measured, using quantitative Western analyses, the levels of MYC_{18}-Tpd3p in strains deleted of *RTS1*, *CDC55*, *PPH21*, *PPH22*, and *PPH21 PPH22*, comparing them with a wild-type strain. Because the levels of Tpd3p in all these strains were essentially the same (our unpublished data), this indicated that the differences in staining patterns of GFP-Tpd3p in the deletion strains must be due to faulty localization processes.

Rts1p Is Dependent on A and C Subunits to Maintain Its Localization

As we had done with GFP-Tpd3p, we asked which PP2A subunits were required for Rts1p-GFP to achieve and maintain normal localization patterns. We first determined whether the loss of Cdc55p had an effect on Rts1p localization and found that the cellular pattern of Rts1p-GFP was both quantitatively and qualitatively similar to that seen in wild-type cells (Figure 8, A and E). In contrast, when we examined *tpd3*Δ cells expressing Rts1p-GFP (MSG100) it was clear that the correct localization of Rts1p was dependent on the presence of Tpd3p. In the *tpd3*Δ strain, Rts1p-GFP lost virtually all of its nuclear, kinetochore/spindle and bud neck localization, and became generally distributed throughout the cytosol in all cell cycle stages (Figure 8, B and E).

As with GFP-Tpd3p, Rts1p-GFP showed partial dependence on Pph21p and Pph22p to maintain its normal localization patterns. The localization of Rts1p-GFP seemed similar in either deletion strain (our unpublished data). When either C subunit was absent, Rts1p-GFP maintained all of its trademark localization patterns, but each pattern was decreased in intensity (Figure 8C). Also, the percentage of cells displaying kinetochore/spindle and bud neck localization patterns was reduced to varying levels (Figure 8E). When both C subunits were deleted, all normal Rts1p localization was affected (Figure 8D). In *pph21*Δ*pph22*Δ (MSG129) cells, Rts1p-GFP appeared as it did in *tpd3*Δ cells (MSG100), i.e., it was generally distributed throughout cells in all cell cycle stages. The percentage of cells exhibiting the trademark localization patterns was reduced to <5% (Figure 8E). Thus, for Rts1p to accumulate at kinetochores and the bud neck, the formation of a complete heterotrimer is required.

As before, we examined the concentration of Rts1p-MYC_{18} in various strains lacking PP2A subunits to determine whether the Rts1p-GFP localization changes in deletion strains were due to a change in Rts1p concentration. *RTS1-MYC*$_{18}$ was expressed on a *CEN* plasmid in *rts1*Δ (YS96), *rts1*Δ*tpd3*Δ (AS11), *rts1*Δ*cdc55*Δ (HFY3), *rts1*Δ*pph21*Δ (AS3), *rts1*Δ*pph22*Δ (AS5), and *rts1*Δ*pph21*Δ*pph22*Δ (AS8) cells. Quantitative Western analysis showed that the concentration of Rts1p-MYC_{18} in each of the deletion strains was indistinguishable (our unpublished data), indicating that the change in localization patterns of Rts1p-GFP in the various deletion strains could not be a consequence of altered Rts1p stability.

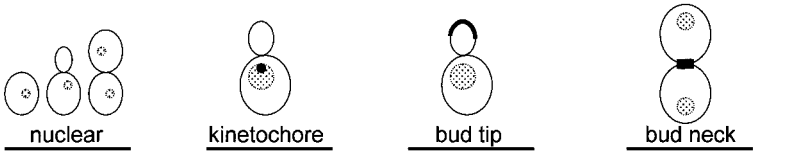

	nuclear	kinetochore	bud tip	bud neck
GFP-Tpd3p	>90%	59% (192/325)	70% (256/365)	61% (199/326)
Rts1p-GFP	>90%	70% (237/336)	N.D.	45% (113/252)
GFP-Cdc55p	>90%	N.D.	61% (149/245)	53% (111/211)

Figure 6. Summary of GFP-PP2A subunit localization patterns. Cells were grown in YPD to early exponential phase at 30°C. Multiple fields of cells were examined and photographs taken of each field. C ells were divided into four classes: nonbudded, small/medium budded, large budded with one nucleus, and large budded with two nuclei (determined by DAPI). Cells in each class were then scored as having or lacking the trademark localization in question. N.D., not detected.

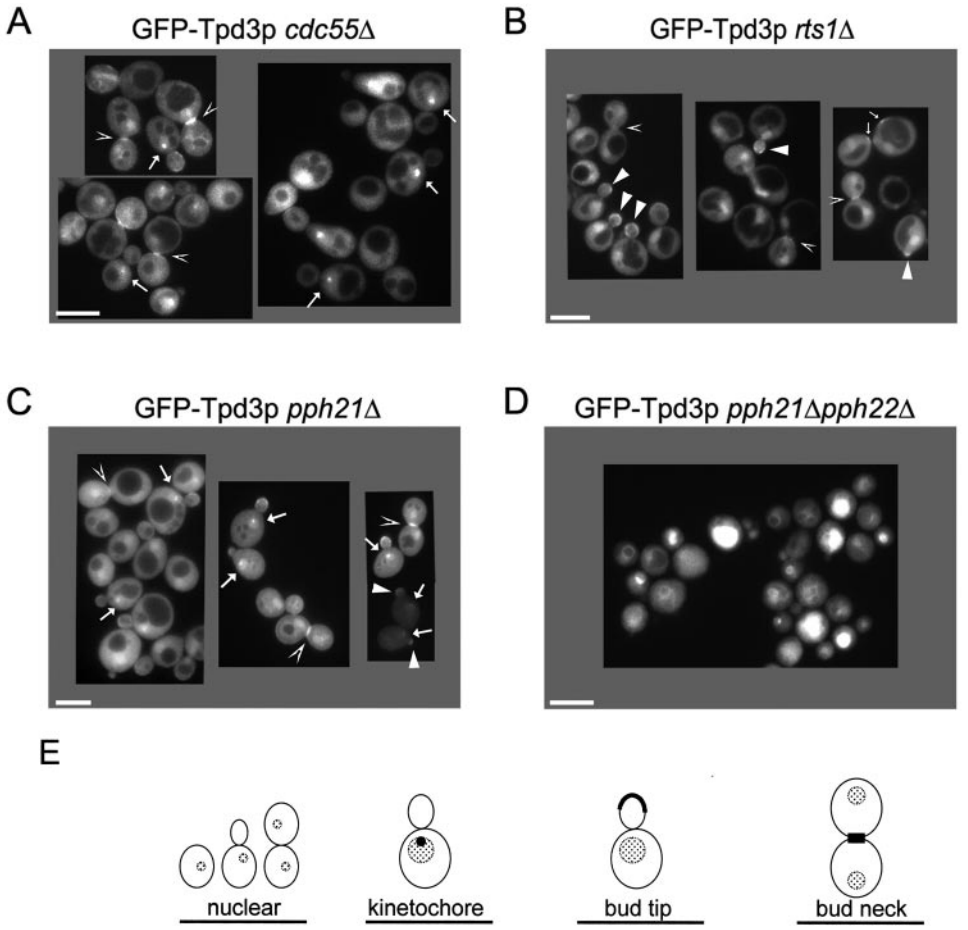

GFP-Tpd3p	>90%	59% (192/325)	70% (256/365)	61% (199/326)
GFP-Tpd3p rts1Δ	>95%$^{+}$	N.D.	37%* (105/285)	31%* (47/152)
GFP-Tpd3p cdc55Δ	>90%*	61% (206/335)	<5%*	42% (121/285)
GFP-Tpd3p cΔrΔ‡	>90%	N.D.	N.D.	N.D.
GFP-Tpd3p pph21Δ	>90%	44%* (189/430)	56%* (202/360)	44%* (109/249)
GFP-Tpd3p pph22Δ	>90%	40%* (167/415)	42%* (122/294)	55%* (186/336)
GFP-Tpd3p 21Δ22Δ	>95%$^{+}$	<1%*	<5%*	<1%*

Figure 7. Localization of GFP-Tpd3p in strains deleted of one or more PP2A subunit encoding genes. MSG81 (A), MSG68 (B), MSG148 (C), and MSG139 (D) cells were grown and examined as described in Figure 2. (E) Quantitation of cells with particular localization patterns was performed as described in Figure 6. N.D., not detected; ‡, *cdc55Δrts1Δ*; *, decreased intensity; $^{+}$, increased intensity.

Cdc55p Can Be Localized Independently of Other PP2A Subunits

To determine whether GFP-Cdc55p was dependent on Tpd3p to maintain its localization, we examined *cdc55Δtpd3Δ* cells (AS13) expressing *GFP-CDC55* on a *CEN* plasmid (MSG369). Surprisingly, cells lacking *TPD3* maintained GFP-Cdc55p at all trademark subcellular locations, albeit at reduced frequencies and intensities (Figure 9, A and F). Nuclear localization of GFP-Cdc55p was greatly reduced (Figure 9F). Similarly, GFP-Cdc55p localization at the bud tip (closed arrowheads) in small/medium budded cells decreased from 61 to 27% and at the bud neck (open arrowheads) of post-telophase cells from 53 to 23% (Figure 9, A and F). Nonetheless, unlike GFP-Tpd3p and Rts1p-GFP, GFP-Cdc55p could still maintain some normal localization whether a heterotrimer could be assembled or not. This would indicate that there is decodable targeting information within Cdc55p itself sufficient for it to achieve and maintain its correct localization at the emerging bud tip and bud neck.

To see whether GFP-Cdc55p localization was in any way affected by the presence of Rts1p, we expressed *GFP-CDC55* from its endogenous promoter on a *CEN* plasmid (MSG369) in *cdc55Δrts1Δ* (HFY3) and *cdc55Δrts1Δtpd3Δ* (AS21) strains. Although deletion of *CDC55* had essentially no effect on Rts1p localization, the reverse was not true. GFP-Cdc55p was still seen at the bud tip and at the bud neck of small/

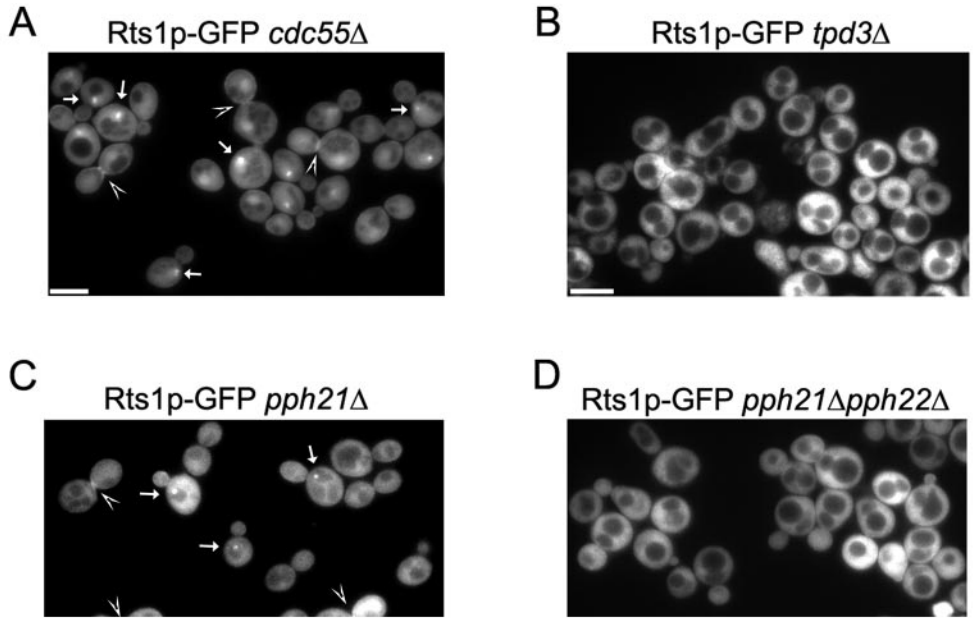

E

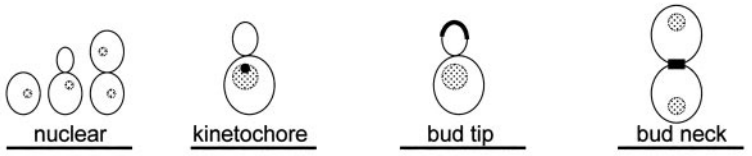

Rts1p-GFP	>90%	70% (237/336)	N.D.	45% (113/252)
Rts1p-GFP cdc55Δ	>90%	60% (184/308)	N.D.	42% (80/192)
Rts1p-GFP tpd3Δ	<5%	N.D.	N.D.	N.D.
Rts1p-GFP pph21Δ	>90%*	52%* (200/385)	N.D.	31%* (61/195)
Rts1p-GFP pph22Δ	>90%*	54%* (233/413)	N.D.	33%* (66/197)
Rts1p-GFP 21Δ22Δ	<5%*	N.D.	N.D.	N.D.

Figure 8. Localization of Rts1p-GFP in strains deleted of one or more PP2A subunit encoding genes. MSG86 (A), MSG100 (B), MSG123 (C), and MSG129 (D) cells were grown and examined as described in Figure 2. (E) Quantitation of cells with particular localization patterns was performed as described in Figure 6. N.D., not detected; *, decreased intensity.

medium budded cells but at considerably reduced frequencies (Figure 9, B, C, and F). Thus, like Rts1p-GFP, GFP-Cdc55p can achieve its normal localization independent of the other B subunit but at a reduced efficiency and frequency. How the absence of Rts1p can affect the relative distribution of Cdc55p in the cell remains to be determined, but we believe it likely to be related to the dramatic asymmetry in the concentrations of these two proteins.

Normal Cdc55p localization also exhibited a partial dependence on the C subunit. In both *pph21*Δ (MSG144) and *pph22*Δ (MSG146) strains, Cdc55p localization seemed the same (our unpublished data); therefore, only *pph21*Δ cells are shown (Figure 9D). GFP-Cdc55p was localized in the nucleus in >90% of all cells (Figure 9F). However, GFP-Cdc55p localization at the bud tip (closed arrowheads) was decreased from 61 to 49% in *pph21*Δ cells and to 36% in *pph22*Δ (Figure 9, D and F). Similarly, GFP-Cdc55p localization to the bud neck (open arrowheads) decreased from 53% in wild-type cells to 37% in *pph21*Δ cells and 36% in *pph22*Δ cells (Figure 9, D and F).

When both C subunits were deleted the percentage of cells exhibiting both bud tip and bud neck localizations decreased to 18 and 20%, respectively (Figure 9, E and F). The GFP-Cdc55p localization that remained at these sites was decreased in intensity compared with wild-type cells, and the bud neck localization was often fragmented and incomplete. Nonetheless, unlike Tpd3p and Rts1p, Cdc55p could be targeted to and accumulate at its normal sites whether or not a catalytic subunit was present in the cell. Thus, the formation of a heterotrimer is unnecessary for localization of Cdc55p. It may well be that the decreased frequency and intensity of localizations seen reflects the necessity of heterotrimer formation for the maintenance of localizations.

As was done with Tpd3p and Rts1p, we then determined the concentration of MYC_{18}-Cdc55p in various PP2A subunit deletion strains: *cdc55*Δ (YS95), *cdc55*Δ*rts1*Δ (HFY21),

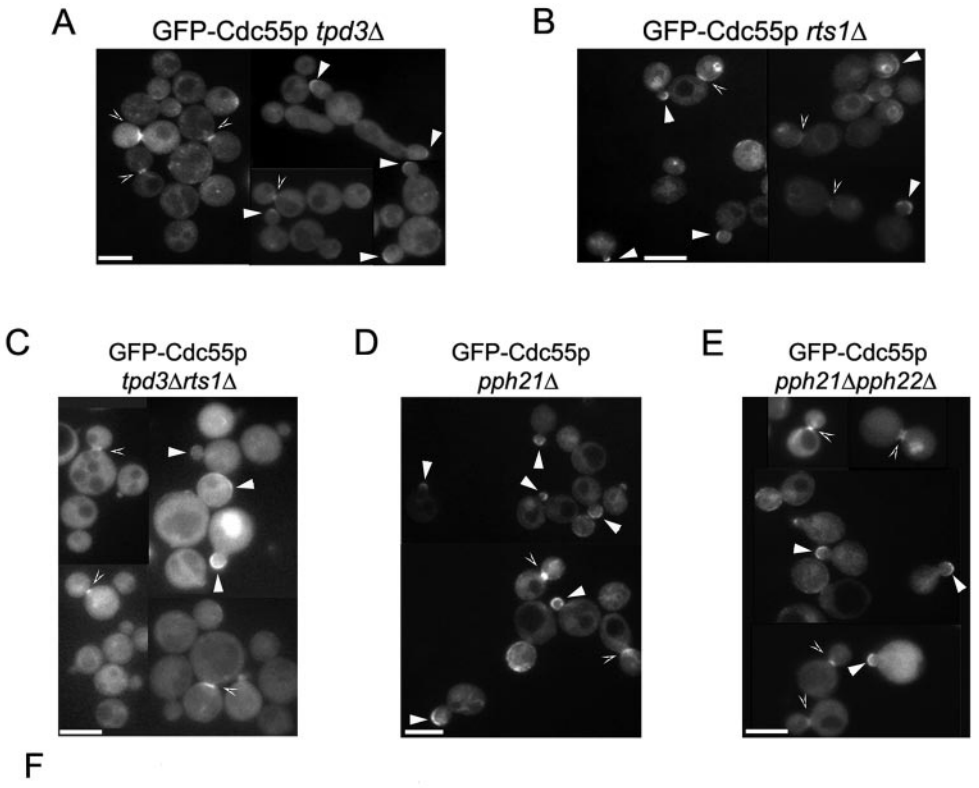

GFP-Cdc55p	>90%	N.D.	61% (149/245)	53% (111/211)
GFP-Cdc55p rts1Δ	>90%$^{+}$	N.D.	31%* (95/307)	29%* (73/251)
GFP-Cdc55p tpd3Δ	<10%	N.D.	27%* (71/262)	23%* (70/302)
GFP-Cdc55p tΔrΔ‡	<10%	N.D.	13%* (37/285)	11%* (26/243)
GFP-Cdc55p pph21Δ	>90%	N.D.	49%* (251/517)	37%* (134/362)
GFP-Cdc55p pph22Δ	>90%	N.D.	36%* (93/256)	36%* (82/230)
GFP-Cdc55p 21Δ22Δ	>90%	N.D.	18%* (36/200)	20%* (45/226)

Figure 9. Localization of GFP-Cdc55p in strains deleted of one or more PP2A subunit encoding genes. AS13 containing pMG369 (A), HFY3 containing pMG369 (B), AS21 containing pMG369 (C), MSG144 (D), and MSG152 (E) cells were grown in YPD or the appropriate selective medium to early exponential phase at 30°C and examined as described in Figure 2. (F) Quantitation of cells was performed as described in Figure 6. N.D., not detected; ‡, *tpd3*Δ*rts1*Δ; *, decreased intensity; $^{+}$, increased intensity.

*cdc55*Δ*tpd3*Δ (AS13), *cdc55*Δ*pph21*Δ (HFY17), *cdc55*Δ*pph22*Δ (HFY19), and *cdc55*Δ*pph21*Δ*pph22*Δ (HFY21). As with the previous two subunits examined, MYC_{18}-Cdc55p concentrations were similar in all strains (our unpublished data). Thus, as with the other two PP2A subunits, the change in localization of GFP-Cdc55p in various PP2A deletion strains was not due to a change in Cdc55p concentration.

DISCUSSION

Quantitative Studies

Although our primary goal in this work was to answer the question of whether PP2A regulatory subunits determined the cellular localization of PP2A holoenzymes, our preliminary analyses of subunit quantitation gave unexpected results. Whereas the cellular levels of all the individual subunits varied little throughout the cell cycle, consistent with the finding that mRNA levels for all the PP2A subunits also vary little (Spellman *et al.*, 1998), they were, surprisingly, far from equimolar. The total number of regulatory subunits (Rts1p plus Cdc55p) per cell was approximately 4 times that of the A subunit (Tpd3p). Similarly, there was 8 times the number of catalytic subunits (Pph21p plus Pph22p) relative to Tpd3p. Clearly, A subunit binding sites must be limiting for both catalytic as well as regulatory subunits. This indicates that some mechanism(s) must exist to regulate the

formation of the various trimers. As Pph21p and Pph22p become incorporated into other complexes (Di Como and Arndt, 1996), the excess of these subunits relative to Tpd3p is understandable, but, again, the control of their partitioning must be regulated in some manner. To date, there have been no reports that indicate that either Rts1p or Cdc55p assemble into other complexes.

The fact that we see no changes in levels of any PP2A subunit proteins in cells unable to express another subunit gene indicates that the stability of the individual proteins is not dependent on whether a particular subunit is or is not in a PP2A complex. Recently, Silverstein *et al.* (2002) reported that in Schneider S2 cells the absence of the A or C subunit led to the degradation of regulatory subunits and the absence of the regulatory subunits led to the degradation of the A and C subunits. In contrast to this report and in agreement with our findings, Wu *et al.* (2000), Evans and Hemmings (2000), and Wei *et al.* (2001) found that subunit stability was not linked to heterotrimer formation in yeast. In addition, our GFP data clearly show that PP2A-GFP fusion proteins persist when PP2A complexes are unable to form. Thus, it seems there is a difference between the two systems with respect to this regulatory mechanism.

In mammalian cells, there is good evidence that a significant pool of AC dimers can be present in the cytosol (Kremmer *et al.*, 1997). We have not addressed experimentally whether such a situation also occurs in *S. cerevisiae.* Although certainly a possibility that needs to be addressed, given the vast excess of B and C subunits relative to Tpd3p in this organism, how such a subpopulation might be maintained would clearly be problematic.

Qualitative Analyses

Our data show that Rts1p and Cdc55p do indeed determine where in the cell Tpd3p, and by inference, Pph21p and Pph22p, accumulate during the cell cycle. Although we could not directly test the effects of B subunit deletion on C subunit localization, the fact that Tpd3p is the only A subunit in *S. cerevisiae*, and that the association of B and C subunits absolutely requires the presence of Tpd3p (Di Como and Arndt, 1996; Shu *et al.*, 1997), its location should define the location of PP2A heterotrimers. Furthermore, the cellular sites at which Rts1p and Cdc55p accumulate are consistent with the mutant phenotypes of *RTS1*-null and *CDC55*-null strains. For example, at elevated temperatures, *rts1*Δ cells accumulate as large budded 2N cells with short spindles, many of which are not correctly oriented (Shu *et al.*, 1997; Hallberg, unpublished data). It was shown (Bloom, personal communication) that these cells display a delayed acquisition of cytoplasmic dynein at their SPBs, consistent with the spindle orientation defect. Similarly, a mutation in *RTS1* is synthetically lethal with a *CIN8* knockout (Hildebrand and Hoyt, unpublished data). Because *CIN8* encodes a microtubule motor protein required for spindle elongation and localizes to kinetochores and the mitotic spindle (Hoyt *et al.*, 1992; He *et al.*, 2001), this correlates with the kinetechore localization of Rts1p. Finally, *rts1*Δ cells are deficient in the splitting of the septin rings just before cell separation (Dobbelaere, Gentry, Hallberg, and Barral, unpublished data), indicating a role for Rts1p in this process. With regard to *CDC55*, cells null for this gene show a random budding pattern (Yang and Hallberg, unpublished data), they display bud morphology defects (Healy *et al.*, 1991), they exhibit septation defects (Healy *et al.*, 1991), septin deposition patterns are aberrant (our unpublished data), and they have deficiencies in degrading Swe1p (Yang *et al.*, 2000). Because Swe1p is thought to be degraded at the bud neck (McMillan *et al.*, 1999; Shulewitz *et al.*, 1999), this again is consistent with bud neck localization of Cdc55p. One Cdc55p localization for which we have yet to identify a mutant phenotype is that at the vacuolar membrane.

In most cases examined, the selective accumulation of a particular subunit absolutely required the presence of a member of each of the other two classes of subunits. For example, selective Tpd3p accumulation at any site required at least one catalytic and one regulatory subunit to be present in the cell. Furthermore, and of primary importance to the hypothesis being tested herein, selective accumulation seen for Tpd3p in either a *CDC55*-null or *RTS1*-null strain reflected only the accumulation sites associated with the particular regulatory subunit still present in the cell. Similarly, Rts1p showed no SPB/kinetechore or bud neck accumulation if either Tpd3p or both of the catalytic subunits were absent. Thus, in all these cases, the capacity to assemble a complete trimer is necessary to achieve selective accumulation at different sites within the cell. Although it may be tempting to hypothesize that the targeting information for these trimers is composed of "bits" from all three subunits, we cannot rule out the alternative explanations that, for example, Rts1p contains the targeting information, but that without an interaction with the other subunits this information is masked, or that targeting of Rts1p takes place but that stable accumulation at a particular site requires a complete trimer. This remains to be resolved.

In contrast, Cdc55p can be targeted to and be accumulated at its normal cellular sites without requiring the presence of either an A subunit or C subunit, albeit that this localization seems not to be as stable as $PP2A_{Cdc55p}$ localization. This means that, theoretically, Cdc55p could be prerecruited to a site in the cell and only later would an AC dimer, should such entities exist in yeast, assemble with it. It remains to be determined whether that, in fact, is what happens in vivo. It may well be that although the targeting information for all trimers resides in their attached regulatory subunits, only in the case of Cdc55p can the regulatory subunit semi-stably accumulate at its normal sites without its associated partners.

Whatever the identity of the *cis*-acting targeting information carried by either of the regulatory subunits, be it necessary and sufficient or just necessary but not sufficient, it must be fairly complex. For instance, with regard to Rts1p, there has to be information that targets Rts1p from the cytosol to the nucleus, to the kinetechore, out of the nucleus, and then to the bud neck. In all these cases, there will presumably be different *trans*-acting proteins with which the regulatory subunits interact. Although most of these will be positive effectors of targeting, it may be that some *trans*-acting factors play a negative role, e.g., they tether Rts1p, thereby preventing an association with Tpd3p. The state of phosphorylation of Rts1p (Shu *et al.*, 1995), which we now know can be regulated during the cell cycle (our unpublished data), may be important in altering its interactions with either of these classes of *trans*-acting factors.

Our localization results, in combination with genetic data currently available or newly generated, should now make it possible to ask whether a particular protein, identified as functionally interacting with Rts1p or Cdc55p, actually colocalizes with either of these B subunits. Given the ever-increasing power of the in situ imaging of cellular proteins, identifying likely potential substrates for particular PP2A holoenzymes by using this approach would seem to us quite promising.

ACKNOWLEDGMENTS

We thank those who kindly supplied strains, plasmids, and antibodies: K. Arndt, J. Bachant, J. Broach, P. Kane, E. Ogris, P. Sorger, and D. Virshup. We thank D. Amberg, S. Erdman, E. Hallberg, W. Jiang, P. Kane, J. Mannion, A. Smuckler, P. Tran, and H. Yang for advice and technical assistance. The critical review of this work and helpful suggestions by the Syracuse University genetics group and UMU-Syracuse/Syracuse University yeast journal club were also greatly appreciated. This work was supported by National Science Foundation grants MCB-9603733 and MCB-0113355.

REFERENCES

Chen, J., Martin, B.L., and Brautigan, D.L. (1992). Regulation of protein serine-threonine phosphatase type-2A by tyrosine phosphorylation. Science *257*, 1261–1264.

Di Como, C.J., and Arndt, K.T. (1996). Nutrients, via the Tor proteins, stimulate the association of Tap42 with type 2A phosphatases. Genes Dev. *10*, 1904–1916.

Donaldson, A.D., and Kilmartin, J.V. (1996). Spc42p: a phosphorylated component of the *S. cerevisiae* spindle pole body (SPD) with an essential function during SPB duplication. J. Cell Biol. *132*, 887–901.

Evans, D.R., and Hemmings, B.A. (2000). Mutation of the C-terminal leucine residue of PP2Ac inhibits PR55/B subunit binding and confers supersensitivity to microtubule destabilization in *Saccharomyces cerevisiae*. Mol. Gen. Genet. *264*, 425–432.

Evans, D.R., and Stark, M.J. (1997). Mutations in the *Saccharomyces cerevisiae* type 2A protein phosphatase catalytic subunit reveal roles in cell wall integrity, actin cytoskeleton organization and mitosis. Genetics *145*, 227–241.

Garcia, A., Cayla, X., and Sontag, E. (2000). Protein phosphatase 2A: a definite player in viral and parasitic regulation. Microbes Infect. *2*, 401–407.

Goh, P.Y., and Kilmartin, J.V. (1993). NDC10: a gene involved in chromosome segregation in *Saccharomyces cerevisiae*. J. Cell Biol. *121*, 503–512.

Guthrie, C., and Fink, G.R. (1991). Guide to yeast genetics and molecular biology. In: Methods in Enzymology, vol. 194, San Diego, CA: Academic Press.

He, X., Asthana, S., and Sorger, P.K. (2000). Transient sister chromatid separation and elastic deformation of chromosomes during mitosis in budding yeast. Cell *101*, 763–775.

He, X., Rines, D.R., Espelin, C.W., and Sorger, P.K. (2001). Molecular analysis of kinetochore-microtubule attachment in budding yeast. Cell *106*, 195–206.

Healy, A.M., Zolnierowicz, S., Stapleton, A.E., Goebl, M., DePaoli-Roach, A.A., and Pringle, J.R. (1991). CDC55, a *Saccharomyces cerevisiae* gene involved in cellular morphogenesis: identification, characterization, and homology to the B subunit of mammalian type 2A protein phosphatase. Mol. Cell. Biol *11*, 5767–5780.

Hoyt, M.A., He, L., Loo, K.K., and Saunders, W.S. (1992). Two *Saccharomyces cerevisiae* kinesin-related gene products required for mitotic spindle assembly. J. Cell Biol. *118*, 109–120.

Janssens, V., and Goris, J. (2001). Protein phosphatase 2A: a highly regulated family of serine/threonine phosphatases implicated in cell growth and signaling. Biochem. J. *353*, 417–439.

Jiang, W., and Hallberg, R.L. (2000). Isolation and characterization of par1(+) and par2(+): two *Schizosaccharomyces pombe* genes encoding B′ subunits of protein phosphatase 2A. Genetics *154*, 1025–1038.

Jiang, Y., and Broach, J.R. (1999). Tor proteins and protein phosphatase 2A reciprocally regulate Tap42 in controlling cell growth in yeast. EMBO J. *18*, 2782–2792.

Jin, Q., Trelles-Sticken, E., Scherthan, H., and Loidl, J. (1998). Yeast nuclei display prominent centromere clustering that is reduced in nondividing cells and in meiotic prophase. J. Cell Biol. *141*, 21–29.

Kaiser, S., Michaelis, S., and Mitchell, A. (1994). Methods in Yeast Genetics. Cold Spring Harbor, NY: Cold Spring Harbor Laboratory.

Kremmer, E., Ohst, K., Kiefer, J., Brewis, N., and Walter, G. (1997). Separation of PP2A core enzyme and holoenzyme with monoclonal antibodies against the regulatory A subunit: abundant expression of both forms in cells. Mol. Cell. Biol. *17*, 1692–1701.

Le Goff, X., Buvelot, S., Salimova, E., Guerry, F., Schmidt, S., Cueille, N., Cano, E., and Simanis, V. (2001). The protein phosphatase 2A B′-regulatory subunit par1p is implicated in regulation of the *S. pombe* septation initiation network. FEBS Lett. *25439*, 1–7.

Lin, F.C., and Arndt, K.T. (1995). The role of *Saccharomyces cerevisiae* type 2A phosphatase in the actin cytoskeleton and in entry into mitosis. EMBO J. *14*, 2745–2759.

McCright, B., Rivers, A.M., Audlin, S., and Virshup, D.M. (1996). The B56 family of protein phosphatase 2A (PP2A) regulatory subunits encodes differentiation-induced phosphoproteins that target PP2A to both nucleus and cytoplasm. J. Biol. Chem. *271*, 22081–22089.

McMillan, J.N., Longtine, M.S., Sia, R.A., Theesfeld, C.L., Bardes, E.S., Pringle, J.R., and Lew, D.J. (1999). The morphogenesis checkpoint in *Saccharomyces cerevisiae*: cell cycle control of Swe1p degradation by Hsl1p and Hsl7p. Mol. Cell. Biol. *19*, 6929–6939.

Meluh, P.B., and Broach, J.R. (1999). Immunological analysis of yeast chromatin. Methods Enzymol. *304*, 414–430.

Millward, T.A., Zolnierowicz, S., and Hemmings, B.A. (1999). Regulation of protein kinase cascades by protein phosphatase 2A. Trends Biochem. Sci. *24*, 186–191.

Minshull, J., Straight, A., Rudner, A.D., Dernburg, A.F., Belmont, A., and Murray, A.W. (1996). Protein phosphatase 2A regulates MPF activity and sister chromatid cohesion in budding yeast. Curr. Biol. *6*, 1609–1620.

Mumby, M.C., and Walter, G. (1993). Protein serine/threonine phosphatases: structure, regulation, and functions in cell growth. Physiol. Rev *73*, 673–699.

Pearson, C.G., Maddox, P.S., Salmon, E.D., and Bloom, K. (2001). Budding yeast chromosome structure and dynamics during mitosis. J. Cell Biol. *152*, 1255–1266.

Pringle, J.R., Preston, R.A., Adams, A.E.M., Stearns, T., Drubin, D.G., Haarer, B.K., and Jones, E.W. (1989). Fluorescence microscopy methods for yeast. In: Methods in Cell Biology, ed. A.M. Tartakoff, San Diego, CA: Academic Press, 357–435.

Ronne, H., Carlberg, M., Hu, G.Z., and Nehlin, J.O. (1991). Protein phosphatase 2A in *Saccharomyces cerevisiae*: effects on cell growth and bud morphogenesis. Mol. Cell. Biol. *11*, 4876–4884.

Rose, M.D., Winston, R., and Heiter, P. (1990). Methods of Yeast Genetics, Cold Spring Harbor, NY: Cold Spring Harbor Laboratory.

Ruediger, R., Roeckel, D., Fait, J., Bergqvist, A., Magnusson, G., and Walter, G. (1992). Identification of binding sites on the regulatory A subunit of protein phosphatase 2A for the catalytic C subunit and for tumor antigens of simian virus 40 and polyomavirus. Mol. Cell. Biol. *12*, 4872–4882.

Sambrook, J., Fritsch, E.F., and Maniatis, T. (1989). Molecular Cloning: A Laboratory Manual, Cold Spring Harbor, NY: Cold Spring Harbor Laboratory.

Schonthal, A.H. (1998). Role of PP2A in intracellular signal transduction pathways. Front. Biosci. *3*, D1262–D1273.

Shu, Y., and Hallberg, R.L. (1995). SCS1, a multicopy suppressor of hsp60-ts mutant alleles, does not encode a mitochondrially targeted protein. Mol. Cell. Biol. *15*, 5618–5626.

Shu, Y., Yang, H., Hallberg, E., and Hallberg, R. (1997). Molecular genetic analysis of Rts1p, a B′ regulatory subunit of *Saccharomyces cerevisiae* protein phosphatase 2A. Mol. Cell. Biol. *17*, 3242–3253.

Shulewitz, M.J., Inouye, C.J., and Thorner, J. (1999). Hsl7 localizes to a septin ring and serves as an adapter in a regulatory pathway that relieves tyrosine phosphorylation of Cdc28 protein kinase in *Saccharomyces cerevisiae*. Mol. Cell. Biol. *19*, 7123–7137.

Silverstein, A.M., Barrow, C.A., Davis, A.J., and Mumby, M.C. (2002). Actions of PP2A on the MAP kinase pathway and apoptosis are mediated by distinct regulatory subunits. Proc. Natl. Acad. Sci. USA *99*, 4221–4226.

Sneddon, A.A., Cohen, P.T., and Stark, M.J. (1990). *Saccharomyces cerevisiae* protein phosphatase 2A performs an essential cellular function and is encoded by two genes. EMBO J. *9*, 4339–4346.

Sontag, E., Nunbhakdi-Craig, V., Bloom, G.S., and Mumby, M.C. (1995). A novel pool of protein phosphatase 2A is associated with microtubules and is regulated during the cell cycle. J. Cell Biol. *128*, 1131–1144.

Spellman, P.T., Sherlock, G., Zhang, M.Q., Iyer, V.R., Anders, K., Eisen, M.B., Brown, P.O., Botstein, D., and Futcher, B. (1998). Comprehensive identification of cell cycle-regulated genes of the yeast *Saccharomyces cerevisiae* by microarray hybridization. Mol. Biol. Cell. *9*, 3273–3297.

Tran, P.T., Marsh, L., Doye, V., Inoue, S., and Chang, R. (2001). A mechanism for the nuclear positioning in fission yeast based on microtubule pushing. J. Cell Biol. *153*, 397–411.

van Zyl, W., Huang, W., Sneddon, A.A., Stark, M., Camier, S., Werner, M., Marck, C., Sentenac, A., and Broach, J.R. (1992). Inactivation of the protein phosphatase 2A regulatory subunit A results in morphological and transcriptional defects in *Saccharomyces cerevisiae.* Mol. Cell. Biol. *12*, 4946–4959.

van Zyl, W.H., Wills, N., and Broach, J.R. (1989). A general screen for mutant of *Saccharomyces cerevisiae* deficient in tRNA biosynthesis. Genetics *123*, 55–68.

Vida, T.A., and Emr, S.D. (1995). A new vital stain for visualizing vacuolar membrane dynamics and endocytosis in yeast. J. Cell Biol. *128*, 779–792.

Virshup, D.M. (2000). Protein phosphatase 2A: a panoply of enzymes. Curr. Opin. Cell Biol. *12*, 180–185.

Wang, Y., and Burke, D.J. (1997). Cdc55p, the B-type regulatory subunit of protein phosphatase 2A, has multiple functions in mitosis and is required for the kinetochore/spindle checkpoint in *Saccharomyces cerevisiae.* Mol. Cell. Biol. *17*, 620–626.

Wei, H., Ashby, D.G., Moreno, C.S., Ogris, E., Yeong, F.M., Corbett, A.H., and Pallas, D.C. (2001). Carboxymethylation of the PP2A catalytic subunit in *Saccharomyces cerevisiae* is required for efficient interaction with the B-type subunits Cdc55p and Rts1p. J. Biol. Chem. *276*, 1570–1577.

Wu, J., Tolstykh, T., Lee, J., Boyd, K., Stock, J.B., and Broach, J.R. (2000). Carboxyl methylation of the phosphoprotein phosphatase 2A catalytic subunit promotes its functional association with regulatory subunits in vivo. EMBO J. *19*, 5672–5681.

Xie, H., and Clarke, S. (1994). Protein phosphatase 2A is reversibly modified by methyl esterification at its C-terminal leucine residue in bovine brain. J. Biol. Chem. *269*, 1981–1984.

Xu, Z., and Williams, B.R. (2000). The B56α regulatory subunit of protein phosphatase 2A is a target for regulation by double-stranded RNA-dependent protein kinase PKR. Mol. Cell. Biol. *20*, 5285–5299.

Yang, H., Jiang, W., Gentry, M., and Hallberg, R.L. (2000). Loss of a protein phosphatase 2A regulatory subunit (Cdc55p) elicits improper regulation of Swe1p degradation. Mol. Cell. Biol. *20*, 8143–8156.